

## Theory of pressure acoustics with thermoviscous boundary layers and streaming in elastic cavities<sup>a)</sup>

Jonas Helboe Joergensen and Henrik Bruus<sup>b)</sup>

Department of Physics, Technical University of Denmark, DTU Physics Building 309, DK-2800 Kongens Lyngby, Denmark

### ABSTRACT:

We present an effective thermoviscous theory of acoustofluidics including pressure acoustics, thermoviscous boundary layers, and streaming for fluids embedded in elastic cavities. By including thermal fields, we thus extend the effective viscous theory by Bach and Bruus [J. Acoust. Soc. Am. **144**, 766 (2018)]. The acoustic temperature field and the thermoviscous boundary layers are incorporated analytically as effective boundary conditions and time-averaged body forces on the thermoacoustic bulk fields. Because it avoids resolving the thin boundary layers, the effective model allows for numerical simulation of both thermoviscous acoustic and time-averaged fields in three-dimensional models of acoustofluidic systems. We show how the acoustic streaming depends strongly on steady and oscillating thermal fields through the temperature dependency of the material parameters, in particular the viscosity and the compressibility, affecting both the boundary conditions and spawning additional body forces in the bulk. We also show how even small steady temperature gradients ( $\sim 1$  K/mm) induce gradients in compressibility and density that may result in very high streaming velocities ( $\sim 1$  mm/s) for moderate acoustic energy densities ( $\sim 100$  J/m<sup>3</sup>).

© 2021 Acoustical Society of America. <https://doi.org/10.1121/10.0005005>

(Received 14 December 2020; revised 30 March 2021; accepted 23 April 2021; published online 26 May 2021)

[Editor: Max Denis]

Pages: 3599–3610

### I. INTRODUCTION

Modeling and simulation are important for designing microscale acoustofluidic systems. Traditionally, most models have been purely mechanical, but some include thermal effects, such as in the studies of the acoustic radiation force acting on suspended microparticles<sup>1–3</sup> and of acoustic streaming in rigid cavities.<sup>4,5</sup>

Here, we focus on acoustic streaming, where recent developments in the field point to the necessity of making a full thermoviscous analysis. Karlsen *et al.*<sup>6</sup> introduced the acoustic body force acting on a liquid governed by solute-induced gradients in the compressibility and density of the liquid. This force has explained the iso-acoustic focusing of microparticles,<sup>7</sup> patterning of concentration profiles,<sup>8</sup> and suppression of acoustic streaming.<sup>9,10</sup> Simultaneously, Bach and Bruus<sup>11</sup> developed the effective theory for pressure acoustics and streaming in elastic cavities, in which the viscous boundary layer was solved analytically and imposed as an effective boundary condition to the bulk field. This model has enabled simulations of cm-sized three-dimensional (3D) acoustofluidic systems,<sup>12,13</sup> with hitherto prohibitive computational costs, and it has provided a deeper insight into the physics of boundary- and bulk-induced streaming, but without thermal effects.<sup>14</sup>

In this work, we combine our previous work on thermoviscous streaming in rigid systems,<sup>5</sup> thermoviscous potential

theory,<sup>3</sup> the theory of pressure acoustics with viscous boundary layers and streaming in curved elastic cavities,<sup>11</sup> and the 3D numerical modeling of acoustofluidic systems using the latter theory,<sup>12</sup> and develop an *effective thermoviscous theory* for a fluid-filled cavity embedded in an elastic solid. The theory includes both steady and acoustic temperature fields for pressure acoustics with thermoviscous boundary layers and for streaming with thermoviscous body forces. In Sec. II, we set up the basic theory and model assumptions. In Secs. III–V, the governing equations and boundary conditions are derived from the theory for the zeroth, first, and second order in the acoustic perturbation, respectively. In Sec. VI, the theory is implemented in a numerical model, which is then used in two examples to show the nature and importance of thermal effects in acoustofluidics. Finally, we conclude in Sec. VII.

### II. BASIC THEORY AND MODEL ASSUMPTIONS

We consider an acoustofluidic device consisting of an elastic solid containing a microchannel filled with a thermoviscous Newtonian fluid and actuated by a piezoelectric transducer at a single frequency in the MHz range. This time-harmonic actuation establishes an acoustic field in the system, which in the fluid, by the internal dissipation and hydrodynamic nonlinearities, results in a time-averaged response that leads to acoustic streaming.

#### A. Governing equations

In this work, unlike prior work,<sup>12</sup> we leave the piezoelectric transducer out of the analysis and only represent it

<sup>a)</sup>This paper is part of a special issue on Theory and Applications of Acoustofluidics.

<sup>b)</sup>Electronic mail: bruus@fysik.dtu.dk, ORCID: 0000-0001-5827-2939.

by an oscillating displacement condition on part of the surface of the elastic solid. The response of the fluid embedded in the elastic solid to this oscillating-displacement boundary condition is controlled by the hydro-, elasto-, and thermodynamic governing equations of the coupled thermoviscous fluid and elastic solid.

The linear elastic solid is described in the Lagrangian picture by the fields of the density  $\rho$ , the displacement  $\mathbf{u}$ , and the temperature  $T$ , as well as the stress tensor  $\boldsymbol{\sigma}$ . Further, for isotropic solids, there are eight material parameters: the longitudinal and transverse sound speeds  $c_{lo}$  and  $c_{tr}$ , the thermal conductivity  $k^{th}$ , the specific heat  $c_p$ , the ratio of specific heats  $\gamma = c_p/c_v$ , the thermal expansion coefficient  $\alpha_p$ , and the isothermal and isentropic compressibilities  $\kappa_s$  and  $\kappa_T = \gamma\kappa_s$ . The velocity field is given as the time derivative of the displacement field  $\mathbf{v}^{sl} = \partial_t \mathbf{u}$ , so no advection occurs, and the governing equations are the transport equations of the momentum density  $\rho \partial_t \mathbf{u}$  and temperature  $T$ ,<sup>3,15</sup>

$$\rho \partial_t^2 \mathbf{u} = \nabla \cdot \boldsymbol{\sigma}, \quad (1a)$$

$$\partial_t T + \frac{(\gamma - 1)}{\alpha_p} \partial_t (\nabla \cdot \mathbf{u}) = \frac{\gamma}{\rho c_p} \nabla \cdot (k^{th} \nabla T), \quad (1b)$$

$$\boldsymbol{\sigma} = -\frac{\alpha_p}{\kappa_T} (T - T_0) \mathbf{I} + \boldsymbol{\tau}, \quad (1c)$$

$$\boldsymbol{\tau} = \rho c_{tr}^2 [\nabla \mathbf{u} + (\nabla \mathbf{u})^T] + \rho (c_{lo}^2 - 2c_{tr}^2) (\nabla \cdot \mathbf{u}) \mathbf{I}, \quad (1d)$$

where superscript ‘‘T’’ indicates a transposed matrix.

The fluid is described in the Eulerian picture by the fields of the density  $\rho$ , the pressure  $p$ , the velocity  $\mathbf{v}$ , the temperature  $T$ , and the energy per mass unit  $\epsilon$ , and by the material parameters as before:  $k^{th}$ ,  $c_p$ ,  $\alpha_p$ ,  $\gamma$ ,  $\kappa_s$ ,  $\kappa_T$ , but with  $c_{tr}$  replaced by the dynamic and bulk viscosity  $\eta$  and  $\eta^b$ . The governing equations are the transport equations for the density of mass  $\rho$ , momentum  $\rho \mathbf{v}$ , and internal energy  $\rho \epsilon$ ,<sup>3,5,16</sup>

$$\partial_t \rho = -\nabla \cdot (\rho \mathbf{v}), \quad (2a)$$

$$\partial_t (\rho \mathbf{v}) = \nabla \cdot (\boldsymbol{\sigma} - \rho \mathbf{v} \mathbf{v}), \quad (2b)$$

$$\partial_t \left( \rho \epsilon + \rho \frac{v^2}{2} \right) = \nabla \cdot \left[ k^{th} \nabla T + \mathbf{v} \cdot \boldsymbol{\sigma} - \rho \mathbf{v} \left( \epsilon + \frac{v^2}{2} \right) \right] + P, \quad (2c)$$

$$\boldsymbol{\sigma} = -p \mathbf{I} + \boldsymbol{\tau}, \quad (2d)$$

$$\boldsymbol{\tau} = \eta [\nabla \mathbf{v} + (\nabla \mathbf{v})^\dagger] + \left( \eta^b - \frac{2}{3} \eta \right) (\nabla \cdot \mathbf{v}) \mathbf{I}. \quad (2e)$$

Here,  $P$  is the external heat power density.

Pressure and temperature are related to the internal energy density by the first law of thermodynamics and to the density by the equation of state,<sup>3,5,17</sup>

$$\rho d\epsilon = (\rho c_p - \alpha_p p) dT + (\kappa_T p - \alpha_p T) dp, \quad (3a)$$

$$d\rho = \rho \kappa_T dp - \rho \alpha_p dT. \quad (3b)$$

The thermodynamics also shows up in the temperature and density dependency<sup>5</sup> of any material parameter  $q$ ,

$$dq = \left( \frac{\partial q}{\partial T} \right)_\rho dT + \left( \frac{\partial q}{\partial \rho} \right)_T d\rho. \quad (4)$$

The temperature sensitivity of each parameter is quantified by the dimensionless quantity  $a_q = 1/\alpha_p q (\partial q / \partial T)_\rho$ ,

$$\begin{aligned} a_\rho &= -1, & a_\eta &= -89, & a_{\eta^b} &= -100, \\ a_{k^{th}} &= 11, & a_{\alpha_p} &= 145, & a_{\kappa_s} &= -10, \end{aligned} \quad (5)$$

where the values are for water at  $T = 25^\circ\text{C}$ .<sup>5</sup> The temperature dependency of the parameters implies that thermal gradients may induce gradients in, say, density and compressibility. This leads to the appearance of the inhomogeneous acoustic body force  $\mathbf{f}_{ac}$  introduced in acoustofluidics for solute-induced gradients by Karlsen *et al.*<sup>6</sup>

## B. Acoustic actuation and perturbation expansion

Following Ref. 11, we actuate time-harmonically with angular frequency  $\omega$  by a displacement of a surface, so an element at equilibrium position  $s_0$ , at time  $t$  will have the position  $\mathbf{s}(s_0, t) = s_0 + s_1(s_0) e^{-i\omega t}$ . For models containing only a fluid, the displacement will be on the fluid boundary, whereas for models containing both a fluid and a solid domain, the actuation is on the solid boundary. For models including the piezoelectric transducer driving the system, the actuation parameter is the applied voltage.<sup>12</sup> However, this is not included in this work.

The acoustic response to the actuation parameter  $s_1$  is linear, and the resulting fields will be complex fields  $Q_1(\mathbf{r}) e^{-i\omega t}$ , the so-called first-order fields with subscript 1. The non-linearity of the governing equation results in higher order responses to the actuation. We are only interested in the time-averaged second-order response and define  $Q_2(\mathbf{r}) = \langle Q_2(\mathbf{r}, t) \rangle = (\omega/2\pi) \int_0^{2\pi/\omega} Q_2(\mathbf{r}, t) dt$ . A time-average of a product of two first-order fields is also a second-order term, written as  $\langle A_1 B_1 \rangle = (1/2) \text{Re}[A_1 B_1^*]$ , where the asterisk denote complex conjugation. Thus, a given field  $Q(\mathbf{r}, t)$  in the model, such as density  $\rho$ , temperature  $T$ , pressure  $p$ , velocity  $\mathbf{v}$ , displacement  $\mathbf{u}$ , and stress  $\boldsymbol{\sigma}$ , is written as the sum of the unperturbed field, the acoustic response, and the time-averaged response,

$$Q(\mathbf{r}, t) = Q_0(\mathbf{r}) + Q_1(\mathbf{r}) e^{-i\omega t} + Q_2(\mathbf{r}). \quad (6)$$

Similarly, through their dependency on temperature and density, all material parameters, such as thermal conductivity  $k^{th}$ , compressibility  $\kappa$ , and (for liquids) viscosity  $\eta$ , are written as exemplified by the viscosity,

$$\eta(\mathbf{r}, t) = \eta_0(T_0) + \eta_1(T_1, \rho_1) e^{-i\omega t} + \eta_2(T_2, \rho_2), \quad (7a)$$

$$\eta_1(T_1, \rho_1) = \left( \frac{\partial \eta}{\partial T} \right)_{T_0} T_1(\mathbf{r}) + \left( \frac{\partial \eta}{\partial \rho} \right)_{T_0} \rho_1(\mathbf{r}), \quad (7b)$$

$$\eta_2(T_2, \rho_2) = \left(\frac{\partial \eta}{\partial T}\right)_{T_0} T_2(\mathbf{r}) + \left(\frac{\partial \eta}{\partial \rho}\right)_{T_0} \rho_2(\mathbf{r}). \quad (7c)$$

### C. Separation of length scales

Acoustofluidic systems exhibit dynamics on two length-scales, set by the acoustic wavelength and the thermoviscous boundary layer width. The boundary conditions on the temperature, heat flux, velocity, and stress at a fluid-solid interface result in the appearance of a thermal boundary layer (in fluids and solids) of width  $\delta_t$  and in a viscous boundary layer (in fluids only) of width  $\delta_s$ , localized near fluid-solid interfaces. Their dynamically-defined widths, jointly referred to as  $\delta$ , are small compared to a typical device size or wavelength  $d$ , so  $\delta \ll d$ ,<sup>3</sup>

$$\delta_s = \sqrt{\frac{2\nu_0}{\omega}}, \quad \delta_t = \sqrt{\frac{2D_0^{\text{th}}}{(1-X)\omega}} \approx \sqrt{\frac{2D_0^{\text{th}}}{\omega}}, \quad (8)$$

where  $X=0$  for fluids and  $X = (\gamma - 1)(4c_{\text{tr}}^2/3c_{\text{lo}}^2) \leq 0.01$  for solids,  $\nu_0 = (\eta_0/\rho_0)$ , and  $D_0^{\text{th}} = k_0^{\text{th}}/\rho_0 c_{p0}$ . Typically,  $\delta_t \lesssim \delta_s \lesssim 500$  nm, which is more than two orders of magnitude smaller than  $d \sim 100$   $\mu\text{m}$ . In this paper, the various fields are decomposed into a bulk field ( $d$ ) and a boundary-layer field ( $\delta$ ) that are connected by the boundary conditions. In Fig. 1, this decomposition is sketched near the fluid-solid boundary for the acoustic temperature field  $T_1$ . Also shown are the boundary-layer widths  $\delta_s$  and  $\delta_t$  together with the instantaneous position  $s(t) = s_0 + s_1(s_0, t)$  of the oscillating boundary.

### D. Boundary conditions

In the usual Lagrangian picture,<sup>11</sup> an element with equilibrium position  $s_0$  in an elastic solid has at time  $t$  the

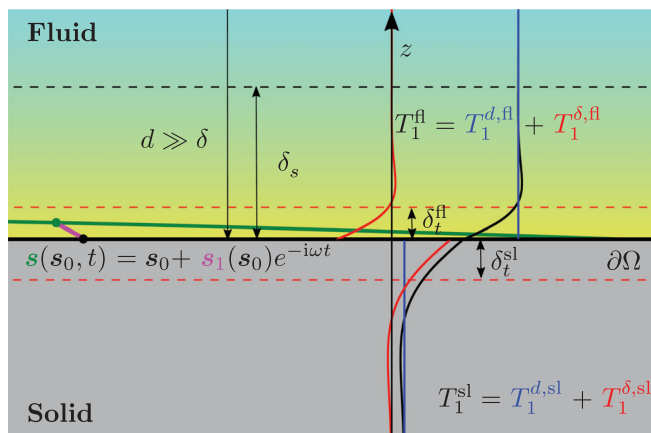


FIG. 1. (Color online) Sketch of the fields at the fluid-solid interface.  $s_0$  is the equilibrium position of the interface  $\partial\Omega$ ,  $s_1$  the time-dependent displacement away from  $\partial\Omega$ , and  $s = s_0 + s_1$  the instantaneous position. The dashed lines represent the viscous and thermal boundary-layer widths  $\delta_s$  (black) and  $\delta_t$  (red) in the solid and fluid.  $\delta$  without a subscript refers to either  $\delta_s$  or  $\delta_t$ , and  $d$  refers to the bulk lengthscale, so  $\delta_t \lesssim \delta_s \sim \delta \ll d$ . The temperature  $T_1^{\text{sl}}$  (black) is the sum of a bulk field  $T_1^{d,\text{sl}}$  (blue) and a boundary-layer field  $T_1^{\delta,\text{sl}}$  (red).

position  $s(s_0, t) = s_0 + s_1(s_0)e^{-i\omega t}$  and velocity  $\mathbf{V}^0 = \partial_t s = \mathbf{V}_1^0(s_0)e^{-i\omega t}$  with  $\mathbf{V}_1^0(s_0) = -i\omega s_1(s_0)$ . On the solid-fluid interface, the no-slip condition applies, so the velocity of the solid wall at a given time and position must equal the Eulerian-picture fluid velocity  $\mathbf{v}^{\text{fl}}$ ,

$$\mathbf{v}^{\text{fl}}(s_0 + s_1 e^{-i\omega t}, t) = \mathbf{V}_1^0(s_0) e^{-i\omega t}. \quad (9)$$

This boundary condition must be obeyed separately for the first- and second-order fields (subscript 1 and 2, respectively), so a Taylor expansion yields<sup>11</sup>

$$\mathbf{v}_1(s_0) = \mathbf{V}_1^0(s_0), \quad (10a)$$

$$\mathbf{v}_2(s_0) = -\langle (s_1 \cdot \nabla) \mathbf{v}_1 \rangle|_{s_0} = -\frac{1}{\omega} \langle (i\mathbf{V}_1^0 \cdot \nabla) \mathbf{v}_1 \rangle|_{s_0}. \quad (10b)$$

At position  $s_0$  on the fluid-solid interface with surface normal  $\mathbf{n}$ , also the stress  $\boldsymbol{\sigma} = \boldsymbol{\sigma}_1 + \boldsymbol{\sigma}_2$  must be continuous in the first- and second-order contributions  $\boldsymbol{\sigma}_1$  and  $\boldsymbol{\sigma}_2$  separately,

$$\boldsymbol{\sigma}_1^{\text{sl}}(s_0) \cdot \mathbf{n} = \boldsymbol{\sigma}_1^{\text{fl}}(s_0) \cdot \mathbf{n}, \quad (11a)$$

$$\boldsymbol{\sigma}_2^{\text{sl}}(s_0) \cdot \mathbf{n} = \boldsymbol{\sigma}_2^{\text{fl}}(s_0) \cdot \mathbf{n} + \langle (s_1 \cdot \nabla) \boldsymbol{\sigma}_1^{\text{fl}}(s_0) \cdot \mathbf{n} \rangle|_{s_0}. \quad (11b)$$

Here, the thermal effects enter through the temperature dependency of the viscosity parameters  $\eta$  and  $\eta^b$ , see Eqs. (2d) and (7).

Similarly, the temperature  $T = T_0 + T_1 + T_2$  must be continuous across the solid-fluid interface in each order separately,

$$T_i^{\text{sl}}(s_0) = T_i^{\text{fl}}(s_0), \quad i = 0, 1, \quad (12a)$$

$$T_2^{\text{sl}}(s_0) = T_2^{\text{fl}}(s_0) + \langle s_1 \cdot \nabla T_1^{\text{fl}} \rangle|_{s_0}. \quad (12b)$$

Also, the heat flux  $\mathbf{n} \cdot (-k^{\text{th}} \nabla T)$  must be continuous across the interface,

$$k^{\text{th,sl}} \mathbf{n} \cdot \nabla T^{\text{sl}}(s_0, t) = k^{\text{th,fl}} \mathbf{n} \cdot \nabla T^{\text{fl}}(s_0 + s_1 e^{-i\omega t}, t), \quad (13)$$

which order by order becomes

$$k_0^{\text{th,sl}} \mathbf{n} \cdot \nabla T_i^{\text{sl}}(s_0) = k_0^{\text{th,fl}} \mathbf{n} \cdot \nabla T_i^{\text{fl}}(s_0), \quad i = 0, 1, \quad (14a)$$

$$\begin{aligned} k_0^{\text{th,sl}} \mathbf{n} \cdot \nabla T_2^{\text{sl}} + k_2^{\text{th,sl}} \mathbf{n} \cdot \nabla T_0^{\text{sl}} + \langle k_1^{\text{th,sl}} \mathbf{n} \cdot \nabla T_1^{\text{sl}} \rangle \\ = k_0^{\text{th,fl}} \mathbf{n} \cdot \nabla T_2^{\text{fl}}(s_0) + \langle k_1^{\text{th,fl}} \mathbf{n} \cdot \nabla T_1^{\text{fl}}(s_0) \rangle \\ + k_2^{\text{th,fl}} \mathbf{n} \cdot \nabla T_0^{\text{fl}}(s_0) + \langle s_1 \cdot \nabla [k_0^{\text{th,fl}} \nabla T_1^{\text{fl}}(s_0)] \cdot \mathbf{n} \rangle \\ + \langle s_1 \cdot \nabla [k_1^{\text{th,fl}} \nabla T_0^{\text{fl}}(s_0)] \cdot \mathbf{n} \rangle. \end{aligned} \quad (14b)$$

### E. Range of validity of the model

We briefly discuss the range of validity imposed by the main assumptions. First, perturbation theory is valid when lower-order terms are much larger than and unaffected by higher-order terms, say,  $\rho_0 \gg |\rho_1|$  and  $|\mathbf{v}_1| \gg |\mathbf{v}_2|$ , and

when the latter can be neglected in the governing equations. For example, zeroth-order heat Eq. (16) is only valid if the timescale for advective heat transport  $t_{adv} = d_t/|v_2|$  is much longer than that of diffusion  $t_{dif} = d_t^2/D_0^{th}$  in a system with characteristic length  $d_t$ . For  $d_t = 1$  mm this requires  $|v_2| \ll (D_0^{th}/d_t) \approx 150 \mu\text{m/s}$ .

Second, due to low oscillatory advection, we assume  $\nabla \cdot (q_0 v_1) \approx q_0 \nabla \cdot v_1$ , where  $q_0$  is a parameter of the fluid. This requires  $|q_0 \nabla \cdot v_1| \gg |\nabla q_0 \cdot v_1|$ . By using the parameter  $a_q$  of Eq. (5), the validity of our theory is limited by

$$|\nabla T_0| \ll \left| \frac{k_c}{a_\eta \alpha_{p0}} \right| \approx 5000 \frac{\text{K}}{\text{mm}}. \quad (15)$$

Here,  $a_\eta$  is used as the viscosity that has the strongest temperature dependency. In conventional acoustofluidic systems,  $|\nabla T_0| \lesssim 50 \text{ K/mm} \ll 5000 \text{ K/mm}$ .

Third, the effective boundary-layer theory requires the boundary-layer width to be much smaller than the bulk wavelength,  $k_0 \delta \ll 1$ , see Sec. II C, which is true for MHz acoustics in water.

### III. ZEROth ORDER: STEADY BACKGROUND FIELDS

Before turning on the acoustics,  $p_0$  is constant and  $v_0 = \mathbf{0}$  in the acoustofluidic system. The temperature  $T_0$  is determined by boundary conditions set by the surroundings and the heat power density  $P_0$  from given sources and sinks.  $T_0$  is governed by the energy conservation [Eq. (2c)] to zeroth order in the acoustic actuation,

$$0 = \nabla \cdot [k_0^{th} \nabla T_0] + P_0. \quad (16)$$

$T_0$  determines the zeroth-order water parameters, such as  $\rho_0(T_0)$  and  $\eta_0(T_0)$ , and thereby affects the resonance frequency and the Q-factor of the acoustofluidic system.

### IV. FIRST ORDER: ACOUSTICS

For the first-order fields, we solve the viscous and thermal boundary layers analytically and use these solutions to derive a set of effective boundary conditions for the bulk fields. The analysis is based on our previous work: the governing equations derived in Refs. 3 and 5, the potential theory derived in Ref. 3, and the effective boundary method derived for viscous but not thermal boundary layers in Ref. 11. The result is a model where we solve for the displacement field  $u_1$  in the solid and for the pressure  $p_1$  in the fluid, and both these bulk fields are subject to the effective boundary conditions that implicitly contain the boundary layers. The temperature  $T_1$  is incorporated through  $p_1$ ,  $u_1$  in the first-order equations and the effective boundary conditions.

#### A. Acoustic equations and potential theory for fluids

The governing equations for the complex-valued acoustic field amplitudes in a fluid are given in Eq. (11) of Ref. 5: the mass continuity equation, the momentum equation, and

the heat equation, which couple together the pressure  $p_1$ , the velocity  $v_1$ , and the temperature  $T_1$ ,

$$-i\omega \alpha_{p0} T_1 + i\omega \kappa_{T0} p_1 = \nabla \cdot v_1, \quad (17a)$$

$$-i\omega \rho_0 v_1 = -\nabla p_1 + \beta \eta_0 \nabla (\nabla \cdot v_1) + \eta_0 \nabla^2 v_1, \quad (17b)$$

$$-i\omega T_1 + i\omega (\gamma - 1) \frac{\kappa_{s0}}{\alpha_{p0}} p_1 = D_0^{th} \nabla^2 T_1, \quad (17c)$$

where  $\beta = (\eta_0^b/\eta_0) - (2/3)$ . Following Ref. 3, these equations are solved using potential theory based on the standard Helmholtz decomposition of the velocity field,  $v_1 = \nabla(\phi_c + \phi_t) + \nabla \times \Psi = v_1^d + v_1^\delta$ , where  $\phi_c$  is the compressional potential,  $\phi_t$  is the thermal potential, and  $\Psi$  is the shear vector potential. At the fluid-solid interface  $|T_1^\delta| \approx |T_1^d|$ , and combining this with  $T_1 = T_1^d + T_1^\delta = [i(\gamma - 1) \omega / \alpha_{p0} c_0^2] \phi_c + (1/\alpha_{p0} D_0^{th}) \phi_t$  with the typical acoustofluidic parameter values inserted, we can deduce  $|\phi_t| \approx (\gamma - 1) (\omega D_0^{th} / c_0^2) |\phi_c| \approx 10^{-8} |\phi_c| \ll |\phi_c|$ . From this follows that  $p_1 \approx i\omega \rho_0 (1 + i\Gamma_s) \phi_c$ , and we replace  $\phi_c$ ,  $\phi_t$ , and  $\Psi$  by  $p_1$ ,  $T_1^\delta$ , and  $v_1^\delta$ ,

$$p_1 \approx i\omega \rho_0 (1 + i\Gamma_s) \phi_c, \quad T_1^\delta = \frac{\phi_t}{\alpha_{p0} D_0^{th}}, \quad v_1^\delta = \nabla \times \Psi. \quad (18)$$

Finally, using the smallness of the damping coefficients,  $\Gamma_s = (1/2)(1 + \beta)(k_0 \delta_s)^2 \ll 1$  and  $\Gamma_t = (1/2)(k_0 \delta_t)^2 \ll 1$ , with  $k_0 = \omega/c$ , approximate solutions to Eq. (17) are obtained from the potentials solving three Helmholtz equations,

$$\nabla^2 p_1 = -k_c^2 p_1, \quad k_c = \frac{\omega}{c_0} (1 + i\Gamma_{0c}^{fl}), \quad (19a)$$

$$\nabla^2 T_1^\delta = -k_t^2 T_1^\delta, \quad k_t = \frac{1 + i}{\delta_t} (1 + i\Gamma_{0t}^{fl}), \quad (19b)$$

$$\nabla^2 v_1^\delta = -k_s^2 v_1^\delta, \quad k_s = \frac{1 + i}{\delta_s}. \quad (19c)$$

Here,  $\Gamma_{0c}^{fl} = [\Gamma_s + (\gamma - 1)\Gamma_t]/2$  and  $\Gamma_{0t}^{fl} = (\gamma - 1)[\Gamma_s - \Gamma_t]/2$  are the resulting damping coefficients, whereas the complex-valued wave numbers  $k_s$  and  $k_t$  reveal the existence of the viscous and thermal boundary layers of thickness  $\delta_s$  and  $\delta_t$ , respectively, see Fig. 1. The full velocity  $v_1$  and temperature  $T_1$  are given by  $p_1$ ,  $v_1^\delta$ , and  $T_1^\delta$  as,

$$v_1 = v_1^d + v_1^\delta = v_1^{d,p} + v_1^{d,T} + v_1^\delta, \quad (20a)$$

$$v_1^{d,p} = \nabla \left[ -i \frac{1 - i\Gamma_s}{\omega \rho_0} p_1 \right], \quad v_1^{d,T} = \nabla \left[ \alpha_{p0} D_0^{th} T_1^\delta \right], \quad (20b)$$

$$T_1 = T_1^d + T_1^\delta, \quad T_1^d = (\gamma - 1) \frac{\kappa_{s0}}{\alpha_{p0}} p_1. \quad (20c)$$

Note that both  $v_1^{d,p}$  and  $v_1^{d,T}$  are gradient fields in the Helmholtz decomposition, but that  $v_1^{d,T}$  despite its superscript ‘‘d’’ is a boundary-layer field. Because  $T_1$  is split into a

bulk and a boundary layer field, the material parameters  $q = q_0 + q_1$  are split similarly. For example, the first-order viscosity  $\eta_1$  introduced in Eq. (7) (and similar for other material parameters) becomes

$$\eta_1 = \partial_T \eta_0 (T_1^d + T_1^\delta) + \partial_\rho \eta_0 (\rho_1^d + \rho_1^\delta) = \eta_1^d + \eta_1^\delta. \quad (21)$$

### B. Acoustic equations and potential theory for solids

For a linear elastic isotropic solid with density  $\rho_0$ , longitudinal sound speed  $c_{lo}$ , and transverse sound speed  $c_{tr}$ , the governing equations are the linearized form of the momentum and heat equation [Eq. (1)] for the displacement field  $\mathbf{u}_1$  and the temperature  $T_1$ ,

$$-\omega^2 \rho_0 \mathbf{u}_1 = -\frac{\alpha_{p0}}{\kappa_{T0}} \nabla T_1 + (c_{lo}^2 - c_{tr}^2) \nabla (\nabla \cdot \mathbf{u}_1) + c_{tr}^2 \nabla^2 \mathbf{u}_1, \quad (22a)$$

$$-i\omega T_1 - i\omega \frac{\gamma - 1}{\alpha_{p0}} \nabla \cdot \mathbf{u}_1 = D_0^{th} \nabla^2 T_1. \quad (22b)$$

In analogy with the fluid, the governing equations for the solid are solved by potential theory, again following Ref. 3. The displacement field is Helmholtz decomposed as  $-i\omega \mathbf{u}_1 = \nabla(\phi_c + \phi_t) + \nabla \times \Psi = -i\omega(\mathbf{u}_1^{lo} + \mathbf{u}_1^{tr})$ , where  $\phi_c$  is the compressional potential,  $\phi_t$  is the thermal potential, and  $\Psi$  is the shear vector potential, and where we have used  $\mathbf{v}_1^{sl} = -i\omega \mathbf{u}_1$ . Using the same approximations as for the fluid, we have  $T_1 = T_1^d + T_1^\delta = [i(\gamma - 1)\omega/\alpha_{p0}c_0^2]\phi_c + (1/\chi\alpha_{p0}D_0^{th})\phi_t$ . We keep  $\phi_c$ , but use  $T_1^\delta = (1/\chi\alpha_{p0}D_0^{th})\phi_t$  instead of  $\phi_t$ , and  $\mathbf{u}_1^{tr} = \nabla \times \Psi$  instead of  $\Psi$ . The solution to Eq. (22) is obtained from the potentials solving the following three Helmholtz equations:

$$\nabla^2 \phi_c = -k_c^2 \phi_c, \quad k_c = \frac{\omega}{c_0} (1 + i\Gamma_{0c}^{sl}), \quad (23a)$$

$$\nabla^2 T_1^\delta = -k_t^2 T_1^\delta, \quad k_t = \frac{1 + i}{\delta_t} (1 + i\Gamma_{0t}^{sl}), \quad (23b)$$

$$\nabla^2 \mathbf{u}_1^{tr} = -k_s^2 \mathbf{u}_1^{tr}, \quad k_s = \frac{\omega}{c_{tr}}. \quad (23c)$$

Here,  $c_0^2 = c_{lo}^2 + (\gamma - 1)/\rho_0\kappa_{T0}$ ,  $\Gamma_{0c}^{sl} = (\gamma - 1)\chi\Gamma_t/2$ , and  $\Gamma_{0t}^{sl} = \gamma^2\Gamma_t/8(1 - X)$  are damping coefficients,  $\delta_t$  and  $\Gamma_t$  are given by Eq. (8),  $\chi = 1 - 4c_{tr}^2/3c^2 \approx 1/2$ , and  $X = (\gamma - 1)4c_{tr}^2/3c^2 \approx (\gamma - 1)/2$ . For a solid, only  $T_1^\delta$  is a dampened field confined to the boundary layer, whereas  $\phi_c$  and  $\mathbf{u}_1^{tr}$  are bulk fields. The transverse waves in fluids and solids are qualitatively different:  $\mathbf{v}_1^\delta$  cannot propagate in a fluid and is restricted to the boundary layer, whereas  $\mathbf{u}_1^{tr}$  can propagate in a solid and is not associated with a boundary layer. The full displacement  $\mathbf{u}_1$  and temperature  $T_1$  are given by  $\phi_c$ ,  $\mathbf{u}_1^{tr}$ , and  $T_1^\delta$  as

$$\mathbf{u}_1 = \mathbf{u}_1^{lo} + \mathbf{u}_1^{tr}, \quad \mathbf{u}_1^{lo} = \frac{i}{\omega} \nabla \phi_c, \quad (24a)$$

$$T_1 = T_1^d + T_1^\delta, \quad T_1^d = \frac{i(\gamma - 1)\omega}{\alpha_{p0}c_0^2} \phi_c. \quad (24b)$$

For most solids, the bulk thermal field  $T_1^d$  is negligible and the displacement can be modelled by Eq. (22a).

The explicit expression for the stress tensor  $\sigma_1^{xl}$  in the fluid ( $xl = fl$ ) and in the solid ( $xl = sl$ ) can be formulated jointly in potential theory as<sup>3</sup>

$$\sigma_1^{xl} = -p_1^{xl} \mathbf{I} + \eta_0^{xl} [(2k_c^2 - k_s^2)\phi_c + (2k_t^2 - k_s^2)\phi_t] \mathbf{I} + \eta_0^{xl} [\nabla \mathbf{v}_1^{sl} + (\nabla \mathbf{v}_1^{sl})^\dagger], \quad (25)$$

where in the solid  $p_1^{sl} = 0$ ,  $\eta_0^{sl} = (i/\omega)\rho_0 c_{tr}^2$ ,  $\mathbf{v}_1^{sl} = -i\omega \mathbf{u}_1$ .

### C. The thermal boundary layer

The temperature fields  $T_1^{\delta,xl}$  in the fluid ( $xl = fl$ ) and the solid ( $xl = sl$ ) are given by Eqs. (19b) and (23b). Following Ref. 11 with  $x$  and  $y$  parallel to the interface and  $z$  perpendicular, an analytical solution can be found using the thin-boundary-layer approximation  $\nabla^2 \approx \partial_z^2$  in these equations in combination with the condition that the field decays away from the boundary,

$$T_1^{\delta,fl}(x, y, z) = T_1^{\delta 0,fl}(x, y) e^{ik_t^{fl}z} \quad \text{for } z > 0, \quad (26a)$$

$$T_1^{\delta,sl}(x, y, z) = T_1^{\delta 0,sl}(x, y) e^{-ik_t^{sl}z} \quad \text{for } z < 0. \quad (26b)$$

The amplitude of the boundary fields  $T_1^{\delta 0,fl}(x, y)$  and  $T_1^{\delta 0,sl}(x, y)$  is determined by the boundary conditions in Eqs. (12a) and (14a) as follows: The normal vector  $\mathbf{n} = -\mathbf{e}_z$  points away from the fluid, so  $\mathbf{n} \cdot \nabla = -\partial_z$ , and we obtain

$$T_1^{\delta 0,fl} = T_1^{\delta 0,sl} - \Delta T_1^{d0}, \quad (27a)$$

$$k_0^{th,fl} \partial_z T_1^{\delta,fl} = k_0^{th,sl} \partial_z T_1^{\delta,sl} \quad \text{for } z = 0, \quad (27b)$$

where  $\Delta T_1^{d0} = -(T_1^{d0,fl} - T_1^{d0,sl})$ . From Eq. (27b), it follows

$$T_1^{\delta 0,fl} = -\frac{k_0^{th,sl} k_t^{sl}}{k_0^{th,fl} k_t^{fl}} T_1^{\delta 0,sl} = -\tilde{Z} T_1^{\delta 0,sl}, \quad (28)$$

where  $\tilde{Z} = Z^{sl}/Z^{fl}$  is the ratio of  $Z = k_0^{th} k_t = \sqrt{k_0^{th} c_{p0} \rho_0}$  of the solid and the fluid, respectively. Combining Eqs. (27a) and (28) leads to the final expression for the boundary-layer fields,

$$T_1^{\delta,fl}(x, y, z) = -\frac{\tilde{Z}}{1 + \tilde{Z}} \Delta T_1^{d0}(x, y) e^{ik_t^{fl}z}, \quad (29a)$$

$$T_1^{\delta,sl}(x, y, z) = +\frac{1}{1 + \tilde{Z}} \Delta T_1^{d0}(x, y) e^{-ik_t^{sl}z}. \quad (29b)$$

### D. The viscous boundary layer

The viscous boundary layer exists only in the fluid since in the solid both  $\mathbf{u}_1^{lo}$  and  $\mathbf{u}_1^{tr}$  are bulk fields. The velocity field

in the fluid is given in Eq. (20a) as  $\mathbf{v}_1 = \mathbf{v}_1^d + \mathbf{v}_1^\delta$ , where  $\mathbf{v}_1^d$  depends on the bulk field  $p_1$  and the boundary field  $T_1^\delta$ . The boundary field  $\mathbf{v}_1^\delta$  is given by the Helmholtz Eq. (19c), to which an analytical solution can be found using the thin-boundary-layer approximation  $\nabla^2 \approx \partial_z^2$  in combination with the condition that the field decays away from the boundary,<sup>11</sup>

$$\mathbf{v}_1^\delta = \mathbf{v}_1^{\delta 0}(x, y) e^{ik_s z}. \quad (30)$$

The amplitude  $\mathbf{v}_1^{\delta 0}$  of the boundary field is determined by the no-slip condition [Eq. (10a)],

$$\mathbf{v}_1^{\delta 0} = \mathbf{V}_1^0 - \mathbf{v}_1^{d0} = -i\omega \mathbf{u}_1^0 - \mathbf{v}_1^{d0}. \quad (31)$$

### E. The effective boundary condition for the velocity

Given the analytical solutions of the three boundary-layer fields, we only need to numerically solve the three bulk fields, namely,  $\phi_c$  and  $\Psi$  in the solid and  $\phi_c$  in the fluid, or equivalently, the displacement  $\mathbf{u}_1$  in the solid and the pressure  $p_1$  in the fluid. Therefore, we set two effective boundary conditions on these bulk fields using the analytical solutions for the boundary-layer fields: One effective boundary condition on the displacement  $\mathbf{u}_1$  in the solid derived from the condition on the stress, and another on the pressure in the fluid.

First, from the no-slip condition [Eq. (10a)], we derive the boundary condition for the first-order pressure field  $p_1$ , which takes the viscous and thermal boundary-layer effects into account through terms with  $k_s$ ,  $k_t$ , and  $T_1^{\delta 0}$ . We express the compressional velocity  $v_{1,z}^{d0,fl}$  on the fluid-solid interface through the no-slip condition [Eq. (31)], then use the incompressibility condition on the boundary-layer velocity,  $ik_s v_{1,z}^{\delta 0,fl} + \nabla \cdot \mathbf{v}_1^{\delta 0,fl} = 0$ , to get rid of the  $z$ -component  $v_{1,z}^{\delta 0,fl}$ , and finally introduce the bulk fields in the fluid,

$$\begin{aligned} v_{1,z}^{d0,fl} &= v_{1,z}^{d0,sl} - v_{1,z}^{\delta 0,fl} = v_{1,z}^{d0,sl} - \frac{i}{k_s} \nabla \cdot \mathbf{v}_1^{\delta 0,fl} \\ &= v_{1,z}^{d0,sl} - \frac{i}{k_s} \nabla \cdot \left[ \mathbf{v}_1^{d0,sl} - \mathbf{v}_1^{d0,fl} \right] \\ &= \left[ v_{1,z}^{d0,sl} - \frac{i}{k_s} \nabla \cdot \mathbf{v}_1^{d0,sl} \right] + \frac{i}{k_s} \left[ \nabla \cdot \mathbf{v}_1^{d,fl} - \partial_z v_{1,z}^{d,fl} \right]_{z=0}. \end{aligned} \quad (32)$$

Combining Eqs. (17a) and (20c), we obtain

$$\nabla \cdot \mathbf{v}_1^d = i \frac{(1 - i\Gamma_s)k_c^2}{\omega\rho_0} p_1 - i\omega\alpha_{p0} T_1^\delta. \quad (33a)$$

Then using Eq. (20a), we write  $v_{1,z}^{d0,fl}$  and  $\partial_z v_{1,z}^{d,fl}$  evaluated at the solid-fluid interface at  $z = 0$ , and arrive at

$$v_{1,z}^{d0,fl} = -\frac{i}{\omega\rho_0} (1 - i\Gamma_s) \partial_z p_1 + \alpha_{p0} D_0^{\text{th}} \partial_z T_1^\delta, \quad (33b)$$

$$\partial_z v_{1,z}^{d,fl} = -\frac{i}{\omega\rho_0} (1 - i\Gamma_s) \partial_z^2 p_1 + \alpha_{p0} D_0^{\text{th}} \partial_z^2 T_1^\delta. \quad (33c)$$

Inserting Eqs. (33) and (10a) into Eq. (32) leads to the final form of the effective boundary condition on  $p_1$ ,

$$\begin{aligned} \partial_z p_1 &= i \frac{\omega\rho_0}{1 - i\Gamma_s} \left( V_{1z}^0 - \frac{i}{k_s} \nabla \cdot \mathbf{V}_1^0 \right) - \frac{i}{k_s} (k_c^2 + \partial_z^2) p_1 \\ &\quad + \frac{i}{k_t} \frac{\alpha_{p0}}{\kappa_{T0}} k_0^2 T_1^{\delta 0} \quad \text{for } z = 0. \end{aligned} \quad (34a)$$

The first two terms on the right-hand were derived by Bach and Bruus,<sup>11</sup> whereas the last term is a new correction due to the thermal boundary layer. For  $T_1^d \approx T_1^\delta$  at  $z = 0$ , this thermal correction is of the order  $[(\gamma - 1)/k_t] k_c^2 p_1$ . We emphasize, that although formulated as an effective boundary condition on the pressure gradient, Eq. (34a) is the no-slip velocity condition.

### F. The effective boundary condition for the stress

Next, using the explicit expressions for  $\sigma_1^{\text{sl}}$  and  $\sigma_1^{\text{fl}}$ , we turn to the stress boundary condition [Eq. (11a)], the continuity of the stress  $\sigma_1$  across the fluid-solid interface,  $\sigma_1^{\text{sl}} \cdot \mathbf{e}_z = \sigma_1^{\text{fl}} \cdot \mathbf{e}_z$ . For the fluid, we use  $k_s \gg k_c$ ,  $|\phi_c| \gg |\phi_t|$ , and  $|\partial_z v_1^\delta| \gg |\nabla v_1^d|$  in Eq. (25), and find

$$\sigma_1^{\text{fl}} \cdot \mathbf{e}_z = -p_1 \mathbf{e}_z + ik_s \eta_0 \left[ \mathbf{v}_1^{d0,sl} + \frac{i}{\omega\rho_0} \nabla p_1 \right]_{s_0}. \quad (34b)$$

For the solid, we neglect in Eq. (25) the derivative  $\partial_{\parallel} \phi_t$  along the surface, as it is a factor  $\Gamma_t = (1/2)(k_0 \delta_t)^2$  smaller than  $\partial_{\parallel} \phi_c$ . The remaining  $\phi_t$ -dependent boundary-layer terms cancel out, leaving only the bulk-term part  $\sigma_1^{d,sl}$  of  $\sigma_1^{\text{sl}}$ . The resulting effective stress boundary condition is

$$\sigma_1^{d,sl} \cdot \mathbf{e}_z = \sigma_1^{\text{fl}} \cdot \mathbf{e}_z. \quad (34c)$$

As the thermal boundary-layer fields do not enter, this expression is identical to the effective boundary condition for the stress derived in Ref. 11.

## V. SECOND ORDER: ACOUSTIC STREAMING

For the second-order fields in the fluid, we follow Eq. (6) and consider only the time averaged fields, namely, the velocity  $\mathbf{v}_2$ , pressure  $p_2$ , and stress  $\sigma_2$ . The temperature field  $T_2$  does not enter the second-order continuity or Navier–Stokes equation, so we drop the heat equation. The first-order temperature field  $T_1$  enters the equations through the material parameters of the fluid,

$$0 = -\nabla \cdot (\rho_0 \mathbf{v}_2) + \dot{\rho}_{\text{ac}}, \quad (35a)$$

$$0 = -\nabla p_2 + \nabla \cdot \tau_2 + \hat{\mathbf{f}}_{\text{ac}}, \quad (35b)$$

$$\tau_2 = \eta_0 \left[ \nabla \mathbf{v}_2 + (\nabla \mathbf{v}_2)^\dagger \right] + \left[ \eta_0^b - \frac{2}{3} \eta_0 \right] (\nabla \cdot \mathbf{v}_2) \mathbf{I}, \quad (35c)$$

$$\mathbf{v}_2^0 = -\frac{1}{\omega} \langle (i\mathbf{V}_1^0 \cdot \nabla) \mathbf{v}_1 \rangle_{r=s_0}. \quad (35d)$$

Here, the excess-density rate-of-change  $\dot{\rho}_{\text{ac}}$  and the acoustic body force  $\hat{\mathbf{f}}_{\text{ac}}$  are defined as time-averaged products of fast

varying first-order fields in the limit  $\rho_0 v_1 \gg \rho_1 v_0$ , which holds for typical acoustofluidic devices,

$$\dot{\rho}_{ac} = -\nabla \cdot \langle \rho_1 v_1 \rangle, \tag{36a}$$

$$\hat{f}_{ac} = \nabla \cdot [-\rho_0 \langle v_1 v_1 \rangle + \tau_{11}], \tag{36b}$$

$$\tau_{11} = \langle \eta_1 [\nabla v_1 + (\nabla v_1)^\dagger] \rangle + \left[ \eta_1^b - \frac{2}{3} \eta_1 \right] (\nabla \cdot v_1) I. \tag{36c}$$

The slowly varying second-order fields are split up in a bulk field (superscript “ $d$ ”) and a boundary field (superscript “ $\delta$ ”) according to their response to the boundary and bulk part of the acoustic force  $\hat{f}_{ac} = \hat{f}_{ac}^d + \hat{f}_{ac}^\delta$ , and they are coupled by the boundary conditions

$$p_2 = p_2^d + p_2^\delta, \quad v_2 = v_2^d + v_2^\delta, \tag{37a}$$

$$\tau_2 = \tau_2^d + \tau_2^\delta, \quad \tau_{11} = \tau_{11}^d + \tau_{11}^\delta. \tag{37b}$$

Note that in contrast to the first-order fields, this is not a Helmholtz decomposition: by definition, a second-order boundary-layer field “ $\delta$ ” contains at least one first-order boundary-layer field. The computation strategy for second-order streaming is similar to the one for first-order acoustics: (1) find analytical solution to the boundary layers, (2) formulate effective boundary conditions, and (3) solve the bulk fields with the effective boundary conditions. This decomposition enables simulations of the bulk fields without resolving the boundary-layer fields.

### A. Short-range boundary-layer streaming

The short-range part “ $\delta$ ” of Eq. (35) is given by the short-range part of the second-order fields as well as all source terms containing at least one boundary-layer field,

$$0 = \nabla \cdot (\rho_0 v_2^\delta) + \dot{\rho}_{ac}^\delta, \tag{38a}$$

$$0 = -\nabla p_2^\delta + \nabla \cdot \tau_2^\delta + \hat{f}_{ac}^\delta, \tag{38b}$$

$$\text{where } v_2^\delta \rightarrow 0 \text{ as } z \rightarrow \infty. \tag{38c}$$

At the boundary, the advection term can be neglected compared to the viscous term because of the large gradients induced by the small lengthscale  $\delta$ . The thermal boundary layer  $T_1^\delta$  and the associated boundary-layer velocity  $v_1^{d,T}$  introduce a correction  $v_2^{\delta,T}$  to the purely viscous boundary-layer term  $v_2^{\delta,p}$  computed in Ref. 11,

$$v_2^\delta = v_2^{\delta,p} + v_2^{\delta,T}. \tag{39}$$

In the parallel component of  $v_2^\delta$ , the pressure field can be neglected because  $\partial_{\parallel} p_2^\delta \ll \eta_0 \partial_z^2 v_2^\delta$ .<sup>11</sup> Thus, combining Eqs. (36b) and (38b), the parallel component of the short-range velocity field  $v_2^{\delta,T}$  obeys

$$\nu_0 \partial_z^2 v_{2,\parallel}^{\delta,T} = \left[ \nabla \cdot \langle v_1^\delta v_1^{d,T} + v_1^{d,T} v_1^\delta + v_1^{d,p} v_1^{d,T} + v_1^{d,T} v_1^{d,p} + v_1^{d,T} v_1^{d,T} \rangle - \frac{1}{\rho_0} \nabla \cdot \tau_{11}^\delta \right]_{\parallel}. \tag{40}$$

Here,  $\tau_{11}^\delta$  depends on  $T_1$  through  $\eta_1(T_1)$ , whereas the velocity  $v_1^{d,T}$ , given in Eq. (20a), depends on the thermal boundary layer  $T_1^\delta$ . From Sec. IV and, in particular, Eqs. (20), (26), and (30), follow the relations  $\nabla \cdot v_1^\delta = 0$ ,  $|v_{1,\parallel}^\delta| \approx |v_{1,\parallel}^d|$ ,  $|v_{1,z}^\delta| \approx (k_c \delta_s) |v_{1,z}^d|$ ,  $|T_1^\delta| \approx |T_1^d|$ ,  $\nabla \cdot v_1^{d,T} \approx (\gamma - 1) \nabla \cdot v_1^{d,p}$ ,  $|v_{1,z}^{d,T}| \approx (\gamma - 1) (k_c \delta_t) |v_{1,z}^{d,p}|$ ,  $|v_{1,\parallel}^{d,T}| \approx (\gamma - 1) (k_c \delta_t)^2 |v_{1,\parallel}^{d,p}|$ , and  $v_1^{d,T} = \alpha_{p0} D_0^{\text{th}} \nabla T_1^\delta$ . To lowest order in  $k_c \delta \ll 1$  (involving  $\partial_z T_1^\delta$  and  $\partial_z v_1^\delta$ , respectively), these relations combined with time averaging  $\text{Re}[a_1] \text{Re}[b_1] = (1/2) \text{Re}[a_1 b_1^*]$  change Eq. (40) to

$$\begin{aligned} \nu_0 \partial_z^2 v_{2,\parallel}^{\delta,T} &= \left[ \left\langle (\partial_z v_1^\delta) v_{1,z}^{d,T} \right\rangle + \left\langle (v_1^\delta + v_1^{d,p}) (\partial_z v_{1,z}^{d,T}) \right\rangle \right. \\ &\quad \left. - \frac{1}{\rho_0} \left( \langle (\partial_z \eta_1^\delta) \partial_z v_1^\delta \rangle + \langle (\eta_1^\delta + \eta_1^d) \nabla^2 v_1^\delta \rangle \right) \right]_{\parallel} \\ &= \frac{1}{2} \text{Re} \left[ \frac{2 \alpha_{p0} D_0^{\text{th}}}{\delta_t^2} \left( \frac{\delta_t + i \delta_s}{\delta_s} v_1^\delta + i v_1^{d,p} \right) T_1^{\delta*} \right. \\ &\quad \left. - \frac{2}{\rho_0 \delta_s^2} \left( \frac{\delta_s + i \delta_t}{\delta_t} \eta_1^\delta + i \eta_1^d \right) v_1^{\delta*} \right]_{\parallel}. \end{aligned} \tag{41}$$

The integration of Eq. (41) after  $z$  twice is facilitated by using the analytical forms [Eqs. (26) and (30)] for  $v_1^{d,T}$ ,  $T_1^\delta$ , and  $v_1^\delta$ , and by noting that in the boundary layer  $\eta_1^d \approx \eta_1^{d0} + z \partial_z \eta_1^d \approx (1 + k_c \delta_s) \eta_1^{d0} \approx \eta_1^{d0}$  and similarly  $v_1^d \approx v_1^{d0}$ ,

$$v_1^\delta = v_1^{\delta 0}(x, y) q(z) \quad \text{with } q(z) = e^{i k_s z}, \tag{42a}$$

$$T_1^\delta = T_1^{\delta 0}(x, y) r(z) \quad \text{with } r(z) = e^{i k_s z}, \tag{42b}$$

$$\eta_1^\delta = \eta_1^{\delta 0}(x, y) r(z), \tag{42c}$$

$$\eta_1^d \approx \eta_1^{d0} \quad \text{and} \quad v_1^{d,p} \approx v_1^{d0,p} \quad \text{for } z \ll d. \tag{42d}$$

Following the procedure of Ref. 11, we introduce the integrals  $I_{ab}^{(n)}$  of the integrand  $a(z) b(z)^*$ , where  $a(z)$  and  $b(z)$  are any of the functions 1,  $q(z)$ , and  $r(z)$ ,

$$\begin{aligned} I_{ab}^{(n)} &= \int^z dz_n \int^{z_n} dz_{n-1} \cdots \int^z dz_1 a(z_1) b(z_1)^* \Big|_{z=0}, \\ I_{ab}^{(n)} &\propto \delta^n \quad \text{with } \delta = \delta_s, \delta_t \text{ and } n = 1, 2, 3, \dots \end{aligned} \tag{43}$$

With this notation, Eq. (41) is easily integrated to give

$$\begin{aligned} v_{2,\parallel}^{\delta 0,T} &= \frac{\alpha_{p0} D_0^{\text{th}}}{\nu_0 \delta_t^2} \text{Re} \left[ \frac{\delta_t + i \delta_s}{\delta_s} I_{qr}^{(2)} v_1^{\delta 0} T_1^{\delta 0*} + i I_{lr}^{(2)} v_1^{d0,p} T_1^{\delta 0*} \right]_{\parallel} \\ &\quad - \frac{1}{\eta_0 \delta_s^2} \text{Re} \left[ \frac{\delta_s + i \delta_t}{\delta_t} I_{rq}^{(2)} \eta_1^{\delta 0} v_1^{\delta 0*} + i I_{lq}^{(2)} \eta_1^{d0} v_1^{\delta 0*} \right]_{\parallel}, \end{aligned} \tag{44a}$$

where the integrals are given by  $I_{ba}^{(n)} = [I_{ab}^{(n)}]^*$  and

$$I_{1r}^{(2)} = -\frac{i}{2}\delta_t^2, \quad I_{1q}^{(2)} = -\frac{i}{2}\delta_s^2, \quad I_{rq}^{(2)} = \frac{i\delta_s^2\delta_t^2}{2(\delta_s + i\delta_t)^2}. \quad (44b)$$

When inserting  $\rho_1^\delta = -\rho_0\alpha_p T_1^\delta$  in the final expression for the thermal correction,  $\mathbf{v}_{2\parallel}^{\delta 0,T}$  becomes

$$\begin{aligned} \mathbf{v}_{2\parallel}^{\delta 0,T} = & -\frac{1}{2\rho_0}\frac{\delta_t^2}{\delta_s^2}\text{Re}\left[\frac{\delta_s}{\delta_s - i\delta_t}\mathbf{v}_1^{\delta 0}\rho_1^{\delta 0*} + \mathbf{v}_1^{d0,p}\rho_1^{\delta 0*}\right]_{\parallel} \\ & -\frac{1}{2\eta_0}\text{Re}\left[\frac{\delta_t}{\delta_t - i\delta_s}\eta_1^{\delta 0}\mathbf{v}_1^{\delta 0*} + \eta_1^{d0}\mathbf{v}_1^{\delta 0*}\right]_{\parallel}, \end{aligned} \quad (45)$$

where two terms are due to the change in density and two to the change in viscosity. The perpendicular part of the short-ranged streaming velocity  $\mathbf{v}_{2z}^{\delta 0,T}$  can be found by integrating the continuity Eq. (35a),  $\partial_z v_{2z}^{\delta 0,T} = -\nabla_{\parallel} \cdot \mathbf{v}_{2\parallel}^{\delta 0,T} - \frac{1}{\rho_0}\nabla \cdot \langle \rho_1 \mathbf{v}_1 \rangle^{\delta 0,T}$ , once with respect to  $z$ ,

$$\mathbf{v}_{2z}^{\delta 0,T} = -\nabla_{\parallel} \cdot \int^z \mathbf{v}_{2\parallel}^{\delta 0,T} dz - \frac{1}{\rho_0} \int^z \nabla \cdot \langle \rho_1 \mathbf{v}_1 \rangle^{\delta 0,T} dz. \quad (46)$$

The term  $\int^z \mathbf{v}_{2\parallel}^{\delta 0,T} dz$  is given by Eq. (44a) by substituting all  $I_{ab}^{(2)}$  by  $I_{ab}^{(3)} \propto I_{ab}^{(2)} \delta$ , so  $|\nabla_{\parallel} \cdot \int^z \mathbf{v}_{2\parallel}^{\delta 0,T} dz| \sim (k_c \delta) |\mathbf{v}_{2\parallel}^{\delta 0}|$ , and  $\int^z \nabla \cdot \langle \rho_1 \mathbf{v}_1 \rangle^{\delta 0,T} dz \approx \int^z \partial_z \langle \rho_1^{\delta} v_{1,z}^{d,p} \rangle dz = \langle \rho_1^{\delta} v_{1,z}^{d,p} \rangle$ . Including pre-factors, we obtain to leading order in  $k_c \delta$ ,

$$\mathbf{v}_{2,z}^{\delta 0,T} = -\frac{1}{2\rho_0}\text{Re}\left[\rho_1^{\delta 0*} v_{1z}^{d0,p}\right]. \quad (47)$$

## B. Bulk field and effective boundary condition

With the short-range boundary-layer streaming term  $\mathbf{v}_2^{\delta 0} = \mathbf{v}_2^{\delta 0,p} + \mathbf{v}_2^{\delta 0,T}$  in place, it is now possible to set up the governing equations and boundary conditions for the second-order bulk acoustic streaming  $\mathbf{v}_2^d$ ,

$$0 = \nabla \cdot (\rho_0 \mathbf{v}_2^d) - \dot{\rho}_{ac}^d, \quad (48a)$$

$$0 = -\nabla p_2^d + \nabla \cdot \boldsymbol{\tau}_2^d + \hat{\mathbf{f}}_{ac}^d, \quad (48b)$$

$$\boldsymbol{\tau}_2^d = \eta_0 \left[ \nabla \mathbf{v}_2^d + (\nabla \mathbf{v}_2^d)^{\dagger} \right] + \beta \eta_0 (\nabla \cdot \mathbf{v}_2) \mathbf{I}, \quad (48c)$$

$$\mathbf{v}_2^{d0} = -\mathbf{v}_2^{\delta 0} - \frac{1}{\omega} \langle (i\mathbf{V}_1^0 \cdot \nabla) \mathbf{v}_1 \rangle|_{r=s_0}. \quad (48d)$$

Here,  $\dot{\rho}_{ac}^d$  and  $\hat{\mathbf{f}}_{ac}^d$  are the bulk terms in Eq. (36). In the mass-conservation equation,  $\nabla \cdot \mathbf{v}_2^d$  becomes

$$\nabla \cdot \mathbf{v}_2^d = -\frac{\nabla \cdot \langle \rho_1^d \mathbf{v}_1^{d,p} \rangle}{\rho_0} = \Gamma \frac{k_0 |\mathbf{v}_1^{d,p}|^2}{2c_0}. \quad (49)$$

Each term of  $\nabla \cdot \mathbf{v}_2^d$  scales as  $(k_0/c_0) |\mathbf{v}_1^{d,p}|^2 \gg (1/2) \Gamma (k_0/c_0) |\mathbf{v}_1^{d,p}|^2$ , so  $(1/\rho_0) \nabla \cdot \langle \rho_1^d \mathbf{v}_1^{d,p} \rangle$  is negligible compared to the individual terms in  $\nabla \cdot \mathbf{v}_2^d$ . We thus conclude that

$\nabla \cdot \mathbf{v}_2^d = 0$ , and that the streaming flow is incompressible. The acoustic body force  $\hat{\mathbf{f}}_{ac}^d$  may be expressed as follows, where  $\nabla \rho_0$  and  $\nabla \kappa_{s0}$  unlike in previous work<sup>6,9</sup> can be induced by temperature gradients:

$$\hat{\mathbf{f}}_{ac}^d = -\nabla \cdot \langle \rho_0 \mathbf{v}_1^{d,p} \mathbf{v}_1^{d,p} \rangle + \nabla \cdot \boldsymbol{\tau}_{11}^d \quad (50a)$$

$$\begin{aligned} & = -\nabla \langle \mathcal{L}_{ac}^d \rangle + \frac{1}{4} |\mathbf{v}_1^{d,p}|^2 \nabla \rho_0 + \frac{1}{4} |p_1|^2 \nabla \kappa_{s0} \\ & \quad - \frac{\Gamma \omega}{c_0^2} \langle \mathbf{v}_1^d p_1 \rangle + \nabla \cdot \boldsymbol{\tau}_{11}^d. \end{aligned} \quad (50b)$$

The gradient force  $-\nabla \langle \mathcal{L}_{ac}^d \rangle$  of the Lagrangian  $\langle \mathcal{L}_{ac}^d \rangle = (1/4) \kappa_{s0} |p_1|^2 - (1/4) \rho_0 |\mathbf{v}_1^d|^2$  does not induce streaming.<sup>11,18</sup> The next two terms form the inhomogeneous acoustic body force spawned by gradients in the density  $\rho_0$  and in the compressibility  $\kappa_{s0}$ .<sup>6</sup> The subsequent Eckart-streaming force term is important for either large systems or for rotating acoustic waves where  $\mathbf{v}_1^d$  and  $p_1$  have significant in-phase components.<sup>14</sup> The last contribution  $\nabla \cdot \boldsymbol{\tau}_{11}^d$  is due to the temperature-dependent viscosity,  $\eta_1^d = a_\eta \eta_0 \alpha_p T_1^d = a_\eta (\gamma - 1) \eta_0 \kappa_{s0} p_1$ . Using  $\mathbf{v}_1^{d,p} \approx -i(1/\omega \rho_0) \nabla p_1$  as well as  $\nabla \cdot [\nabla \mathbf{v}_1^{d,p} + (\nabla \mathbf{v}_1^{d,p})^{\dagger}] = 2\nabla (\nabla \cdot \mathbf{v}_1^{d,p}) = -2k_c^2 \mathbf{v}_1^{d,p}$ ,  $\nabla \eta_1^d = a_\eta \eta_0 (\gamma - 1) (ik_c/c_0) \mathbf{v}_1^{d,p}$ , and  $\langle \eta_1 (\nabla \cdot \mathbf{v}_1^{d,p}) \rangle \propto \langle p_1 (ip_1) \rangle = 0$ , we reduce  $\nabla \cdot \boldsymbol{\tau}_{11}^d$  to

$$\begin{aligned} \nabla \cdot \boldsymbol{\tau}_{11}^d = & 2(\gamma - 1) a_\eta \eta_0 \frac{\omega^2}{c_0^2} \\ & \times \left[ \left\langle \left( \frac{i}{\omega} \mathbf{v}_1^{d,p} \cdot \nabla \right) \mathbf{v}_1^{d,p} \right\rangle - \kappa_{s0} \langle \mathbf{v}_1^{d,p} p_1 \rangle \right]. \end{aligned} \quad (51)$$

Here, the first and second term involve the Stokes drift and the classical Eckart attenuation [Eq. (50b)], respectively. Now, collecting the results [Eqs. (49)–(51)], the governing equations [Eq. (48a)–(48c)] of the acoustic streaming become

$$0 = \nabla \cdot \mathbf{v}_2^d, \quad (52a)$$

$$0 = -\nabla [p_2^d - \langle \mathcal{L}_{ac}^d \rangle] + \eta_0 \nabla^2 \mathbf{v}_2^d + \hat{\mathbf{f}}_{ac}^d, \quad (52b)$$

$$\begin{aligned} \hat{\mathbf{f}}_{ac}^d = & -\frac{1}{4} |\mathbf{v}_1^{d,p}|^2 \nabla \rho_0 - \frac{1}{4} |p_1|^2 \nabla \kappa_{s0} \\ & + \left[ 1 - \frac{2a_\eta (\gamma - 1)}{\beta + 1} \right] \frac{\Gamma \omega}{c_0^2} \langle \mathbf{v}_1^{d,p} p_1 \rangle \\ & + 2a_\eta \eta_0 (\gamma - 1) \frac{\omega}{c_0^2} \langle i \mathbf{v}_1^{d,p} \cdot \nabla \mathbf{v}_1^{d,p} \rangle. \end{aligned} \quad (52c)$$

Here, the Lagrangian density  $\langle \mathcal{L}_{ac}^d \rangle$  is merged with  $p_2^d$  as an excess pressure. Since  $\nabla \langle \mathcal{L}_{ac}^d \rangle$  is orders of magnitude larger than  $\hat{\mathbf{f}}_{ac}^d$ , its merging with  $\nabla p_2^d$  renders the numerical simulation more accurate,<sup>18</sup> and makes it possible to use a coarser mesh in the bulk of the fluid domain.<sup>11</sup> The term  $-[2a_\eta (\gamma - 1)]/(\beta + 1) \approx 0.44$  leads to an increase in the bulk-driven Eckart streaming by 44% compared to a purely viscous model. The last term is due

to gradients in the viscosity  $\eta_1^d$ , so a fluid particle oscillating  $\mathbf{s}_1 = (i/\omega)\mathbf{v}_1^{d,p}$  experiences a varying viscosity during its oscillation period.

Finally, the thermal corrections to the boundary condition [Eq. (48d)] stem from  $\mathbf{v}_2^{\delta_0,T}$  in the boundary-layer velocity  $\mathbf{v}_2^{\delta_0} = \mathbf{v}_2^{\delta_0,p} + \mathbf{v}_2^{\delta_0,T}$ , see Eqs. (45) and (47), and from  $\mathbf{v}_1^{d,T}$  in  $\mathbf{v}_1 = \mathbf{v}_1^\delta + \mathbf{v}_1^{d,p} + \mathbf{v}_1^{d,T}$  in the Stokes drift term  $-(1/\omega) \langle (i\mathbf{V}_1^0 \cdot \nabla)\mathbf{v}_1 \rangle|_{r=s_0}$ . As  $|\mathbf{v}_1^{d,T}| \ll |v_{1z}^{d,T}|$ , then  $\mathbf{V}_1^0 \cdot \nabla \mathbf{v}_1^{d,T} \approx V_{1,z}^0 \alpha_{p0} D_0^{\text{th}} \partial_z^2 T_1^\delta \mathbf{e}_z = (\omega/\rho_0) V_{1,z}^0 (i\rho_1^\delta) \mathbf{e}_z$ ,

$$\frac{1}{\omega} \langle (i\mathbf{V}_1^0 \cdot \nabla)\mathbf{v}_1^{d,T} \rangle|_{r=s_0} = \frac{1}{2\rho_0} \text{Re} \left[ V_{1,z}^0 \rho_1^{\delta_0*} \right] \mathbf{e}_z. \quad (53)$$

In terms of the  $\mathbf{A}$ - and  $\mathbf{B}$ -vector notation of Ref. 11, the boundary condition [Eq. (48d)] for the streaming velocity  $\mathbf{v}_2^d$  is given by the purely viscous terms (superscript “vs”) from Ref. 11 and the thermal corrections (superscript “th”) due to  $\mathbf{v}_2^{\delta_0,T}$ , Eqs. (45) and (47), and  $\mathbf{v}_1^{d_0,T}$ , Eq. (53),

$$\mathbf{v}_2^{d_0} = (\mathbf{A} \cdot \mathbf{e}_x)\mathbf{e}_x + (\mathbf{A} \cdot \mathbf{e}_y)\mathbf{e}_y + (\mathbf{B} \cdot \mathbf{e}_z)\mathbf{e}_z, \quad (54a)$$

with  $\mathbf{A} = \mathbf{A}^{\text{vs}} + \mathbf{A}^{\text{th}}$ ,  $\mathbf{B} = \mathbf{B}^{\text{vs}} + \mathbf{B}^{\text{th}}$ ,

$$\mathbf{A}^{\text{vs}} = -\frac{1}{2\omega} \text{Re} \left[ \mathbf{v}_1^{\delta_0*} \cdot \nabla \left( \frac{1}{2} \mathbf{v}_1^{\delta_0} - i\mathbf{V}_1^0 \right) - i\mathbf{V}_1^{0*} \cdot \nabla \mathbf{v}_1^{d,p} + \left\{ \frac{2-i}{2} \nabla \cdot \mathbf{v}_1^{\delta_0*} + i \left( \nabla \cdot \mathbf{V}_1^{0*} - \partial_z v_{1z}^{d,p*} \right) \right\} \mathbf{v}_1^{\delta_0} \right], \quad (54b)$$

$$\mathbf{A}^{\text{th}} = \frac{1}{2\rho_0 \delta_s^2} \text{Re} \left[ \frac{\delta_s}{\delta_s - i\delta_t} \mathbf{v}_1^{\delta_0} \rho_1^{\delta_0*} + \mathbf{v}_1^{d_0,p} \rho_1^{\delta_0*} \right] + \frac{1}{2\eta_0} \text{Re} \left[ \frac{\delta_t}{\delta_t - i\delta_s} \eta_1^{\delta_0} \mathbf{v}_1^{\delta_0*} + \eta_1^{d_0} \mathbf{v}_1^{\delta_0*} \right], \quad (54c)$$

$$\mathbf{B}^{\text{vs}} = \frac{1}{2\omega} \text{Re} \left[ i\mathbf{v}_1^{d_0,p*} \cdot \nabla \mathbf{v}_1^{d,p} \right], \quad (54d)$$

$$\mathbf{B}^{\text{th}} = \frac{1}{2\rho_0} \text{Re} \left[ \left( \mathbf{v}_1^{d_0,p} - \mathbf{V}_1^0 \right) \rho_1^{\delta_0*} \right]. \quad (54e)$$

The magnitude of the thermal terms are  $(\gamma - 1)a_q$  times the magnitude of the leading viscous terms. For water,  $(\gamma - 1)|a_\eta| \approx 0.9$  and  $(\gamma - 1)|a_\rho| \approx 0.01$  at room temperature, so here, the  $\eta_1$ -terms are important and must be included in acoustofluidic analyses, whereas  $\rho_1$ -terms are negligible. For gases with  $\gamma - 1 \approx 0.4$ , the density terms may be important.

The results in Eqs. (52) and (54) are our main results for the second-order streaming part of the effective thermoviscous theory, and they form the equations that are implemented in our numerical model.

## VI. NUMERICAL IMPLEMENTATION AND EXAMPLES

We implement the effective thermoviscous model in the commercial finite-element software COMSOL Multiphysics.<sup>19</sup> It is validated by comparisons to full

numerical simulations, and two examples of significant thermal effects in acoustofluidic devices are shown. All simulations are done in COMSOL 5.6<sup>19</sup> on a HP-G4 workstation with a processor Intel Core i9-7960X @ 4.20 GHz and with 128 GB ram.

The effective thermoviscous model solver contains three steps: (1) the zeroth-order thermal field, (2) the acoustic pressure and displacement fields, and (3) the stationary streaming fields. The acoustic temperature field  $T_1$  is included analytically and therefore does not increase the numerical workload compared to the purely viscous model. The effective thermoviscous theory allows us to simulate acoustofluidic systems in three dimensions, which has prohibitive numerical costs for the full model.

Following our previous work,<sup>5,6,11,12,20</sup> the governing equations [Eqs. (16), (19), (22a), and (52)] are implemented in COMSOL using the mathematical PDE Module. The surface fields (superscript “0”) are defined only on the fluid-solid interfaces. The effective boundary conditions [Eq. (34)] for  $p_1$  and  $\mathbf{u}_1$  are implemented as weak contributions, whereas the boundary condition in Eq. (54) for  $\mathbf{v}_2^d$  is implemented as a Dirichlet boundary condition. Further details on the implementation of the numerical model in COMSOL are presented in the supplementary material.<sup>21</sup>

### A. Example I: Two-dimensional (2D) streaming in a square channel

The first example is the square channel, which has been studied both experimentally<sup>22–24</sup> and numerically.<sup>22</sup> In a square channel, a rotating acoustic wave can be set up by two perpendicular, out-of-phase standing waves, as analyzed theoretically by Bach and Bruus.<sup>14</sup> We apply the effective thermoviscous model in the fluid domain of the square channel in the 2D  $yz$  cross section with the velocity  $\mathbf{V}_1^0 = V_0 e^{-i\omega t} \mathbf{e}_y$  at the vertical sides  $y = \pm(1/2)W$  and  $\mathbf{V}_1^0 = iV_0 e^{-i\omega t} \mathbf{e}_z$  at the horizontal sides  $z = \pm(1/2)H$ , a rigid-wall model with side length  $H = W = 230 \mu\text{m}$ . The zeroth-order temperature field is set to be constant,  $T_0 = 20 \text{ }^\circ\text{C}$ . We emphasize three main points of the results, shown in Fig. 2: (1) The effective model reduces the computational time and memory requirements significantly. (2) Given that it is 2D, the full model can be simulated, and it agrees with and thus validates the effective model. (3) The thermal corrections strongly influence the streaming flow pattern.

The meshes plotted on top of the pressure field in Fig. 2(a) are the ones needed to obtain an  $L_2$ -norm-convergence<sup>5</sup> of 0.1% for  $p_1$  and 1% for the streaming  $\mathbf{v}_2$  for the full and for the effective model. With computation times of 15 versus 2 s and 130 042 degrees of freedoms versus 1788, the effective model is in this case seven times faster and requires 130 times less memory than the full mode to achieve the same accuracy. Figures 2(b)–2(f) show the resulting streaming  $\mathbf{v}_2$  obtained using different assumptions. Figures 2(e) and 2(f) illustrate that the effective and full models agree, thus validating the former. Figure 2(b) shows how much  $\mathbf{v}_2$  is changed when disregarding all thermal

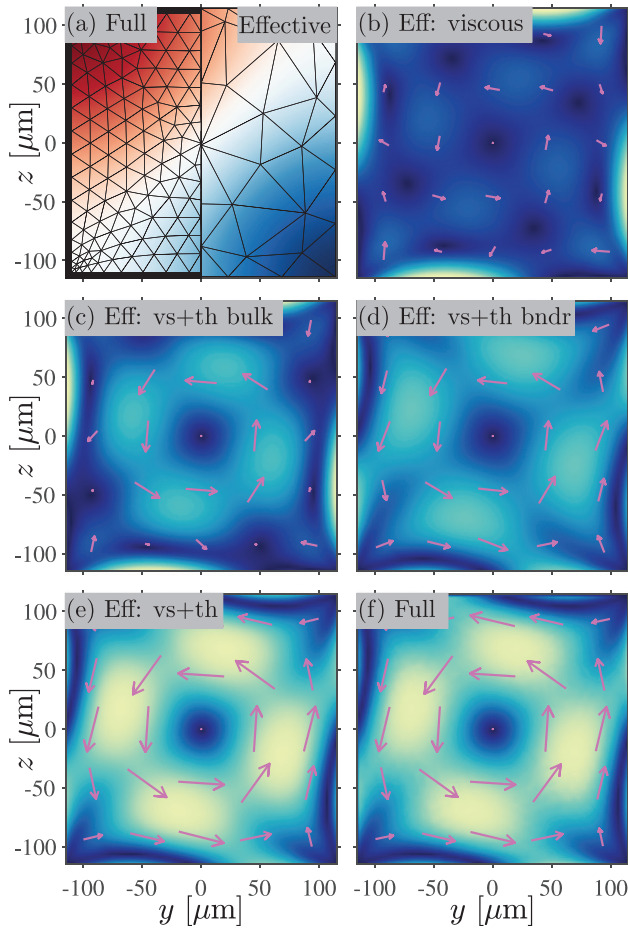


FIG. 2. (Color online) Simulated fields in a square channel with a rotating pressure wave of energy density  $E_{ac} = 19 \text{ J/m}^3$  actuated as described in the text. (a) Color plot of  $p_1$  at time  $t = 0$  from  $-0.4$  (blue) to  $+0.4$  MPa (red), and the mesh used in the full (left) and in the effective (right) thermoviscous model. (b) Vector plot of the streaming velocity  $v_2$  (magenta) and color plot of its magnitude from 0 (dark blue) to  $20 \mu\text{m/s}$  (yellow) [same scale in (b)–(f)] for the effective viscous model without thermal terms. (c)  $v_2$  for the effective viscous model with thermal bulk terms. (d)  $v_2$  for the effective viscous model with thermal boundary terms. (e)  $v_2$  for the complete effective thermoviscous model. (f)  $v_2$  for the full thermoviscous model.

effects as in Ref. 11, whereas Figs. 2(c) and 2(d) illustrate the effect of adding only the thermal bulk effects of Eq. (52), and adding only the thermal correction to the boundary condition of Eq. (54). Clearly, all the thermal effects need to be added, and in this example, they stem from the temperature dependence of the viscosity through  $\eta_1$  in the bulk term [Eq. (50)]  $\nabla \cdot \tau_{11}$  and the boundary term [Eq. (54)]  $A^T$ . Physically, the bulk term strengthens the central streaming roll, whereas the boundary term changes the morphology of the boundary streaming and additionally strengthens the central streaming roll.

### B. Example II: 3D streaming due to thermal fields

The second example is the capillary glass tube widely used as a versatile acoustic trap in many experimental studies.<sup>23–26</sup> Inside the tube, in the region above the piezoelectric transducer, a characteristic streaming flow pattern containing four horizontal flow rolls is established.<sup>25</sup> This

pattern cannot be explained in numerical modeling<sup>20,27</sup> in terms of boundary-driven streaming or classical bulk Eckart streaming; however, here we argue, based on our thermoacoustic simulation results, that thermal effects are responsible for this streaming pattern. This result is important as the streaming pattern is used to lead nanoparticles into the central region, where they are trapped by larger seed particles.

The 3D model, see Fig. 3, is similar to device C1 in our previous work:<sup>20</sup> a glass capillary tube of width  $W = 2 \text{ mm}$  and height  $H = 0.2 \text{ mm}$ , actuated from below in its central region by a piezoelectric transducer. The temperature is set to  $T_{air} = 25 \text{ }^\circ\text{C}$  at  $x = L_{end}$  and to zero flux on all other outer surfaces except on the transducer. For simplicity, the transducer is represented by a (red) region of width  $W_{PZT}$ , length  $L_{PZT} = 1.16 \text{ mm}$  on the glass surface, with a given oscillatory displacement  $\mathbf{u} = \mathbf{u}_{PZT}e^{-i\omega t}$  and steady temperature<sup>28</sup>  $T = T_{air} + T_{PZT}$ , where  $\mathbf{u}_{PZT} = u_0 \mathbf{e}_z$  with  $u_0 = 0.25 \text{ nm}$  and  $T_{PZT} = 1.5 \text{ }^\circ\text{C}$ . We exploit the  $xz$  and  $yz$  symmetry planes and simulate only a quarter of the system. To simulate an infinitely long channel, we use a perfectly matched layer (PML) to avoid reflections from the ends.<sup>20,21,29</sup>

The mesh shown in Fig. 3(a) results in an  $L_2$ -norm-convergence<sup>5</sup> of 1% in the pressure  $p_1$  and in the streaming  $v_2$ , and of 3% in the displacement  $\mathbf{u}_1$ . The simulation requires 491.959 degrees of freedom and takes 7 min.

For the steady temperature  $T_0$  shown in Fig. 3(b), we find by inspection a resonance at  $f = 3.898 \text{ MHz}$ , for which the resulting acoustic displacement  $\mathbf{u}_1$  and pressure  $p_1$  are

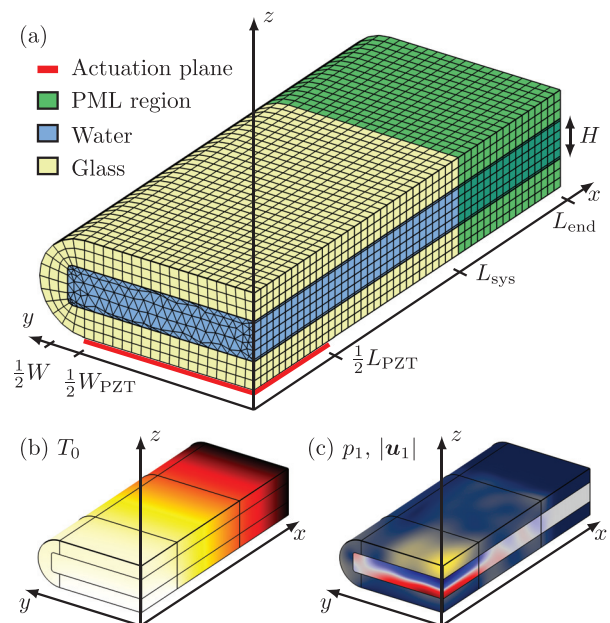


FIG. 3. (Color online) (a) The simulated 3D system (reduced to a quarter by symmetry) consisting of the water (blue), the glass (yellow), and the artificially absorbing PML (green) domains described further in the supplementary material (Ref. 21). Also, shown are the actuation region (red) and the mesh (black). (b) Color plot of the steady temperature  $T_0$  from  $20.0$  (black) to  $21.5 \text{ }^\circ\text{C}$  (yellow). (c) Color plots of the displacement  $|\mathbf{u}_1|$  in the glass from 0 (blue) to  $9.5 \text{ nm}$  (yellow) and the acoustic pressure  $p_1$  in the water from  $-1.6$  (blue) to  $+1.6 \text{ MPa}$  (red). Note the dampening of  $\mathbf{u}_1$  and  $p_1$  in the PML region.

shown in Fig. 3(c).  $T_0$  is inhomogeneous with an almost constant temperature gradient along the tube in the  $x$ -direction, and, in agreement with previous experiments<sup>25</sup> and simulations,<sup>20</sup>  $p_1$  appears as a vertical half-wave resonance localized in the region above the transducer, but stronger in the center than at the sides. Combining the effects of  $p_1$  and the  $T_0$ -dependency of the density  $\rho_0$  and compressibility  $\kappa_{s,0}$ , the acoustic body force [Eq. (52c)] driving the streaming  $v_2$  becomes

$$\begin{aligned} f_{ac}^d &\approx -\frac{1}{4}|v_1|^2 \nabla \rho_0 - \frac{1}{4}|p_1|^2 \nabla \kappa_{s,0} \\ &= -\frac{1}{4}(a_\rho \rho_0 |v_1|^2 + a_\kappa \kappa_{s,0} |p_1|^2) \alpha_{\rho 0} \nabla T_0. \end{aligned} \quad (55)$$

Since by Eq. (5),  $\kappa_s$  has a stronger temperature dependency than  $\rho$ ,  $f_{ac}^d$  is dominated by the  $|p_1|^2$ -term. This results in a body force parallel to  $\nabla T_0$  and strongest in the center, where  $|p_1|$  is maximum.

The numerical simulation result for  $v_2$  is shown in Fig. 4: The characteristic four horizontal flow rolls are clearly seen, the radius of which is determined by the width of the

channel and the width of the actuation as observed by Hammarström *et al.*<sup>25</sup> This phenomenon is explained in terms of the acoustic body force  $f_{ac}^d$ , which pushes the liquid into the center region near the vertical  $xz$ -plane at  $y = 0$ , where it is strongest, accompanied by a back-flow at the edges near  $y = \pm(1/2)W$ , where the body force is weaker. In Fig. 4(a),  $v_2$  is shown in three different horizontal planes. The variation in the flow rolls reflects the  $z$ -dependence of the thermal gradient above the transducer. In Fig. 4(b),  $v_2$  is shown in the full horizontal plane at  $z = 0 \mu\text{m}$ . Note how the four flow roll centers are located near the edge (red lines) of the actuation region. To emphasize the crucial role of the thermal effects, we show in Fig. 4(c) the streaming flow resulting from neglecting all thermal effects: In agreement with previous purely viscous models, but in contrast to experimental observations, the characteristic four-flow-roll pattern does not appear. Another important feature of the thermoviscous streaming is its magnitude. In Fig. 4,  $|v_2| = 50 \mu\text{m/s}$  is obtained with an acoustic energy density of  $E_{ac} = 77 \text{ J/m}^3$ . This is five times larger than the  $10 \mu\text{m/s}$  of the purely viscous streaming, and notably only a factor of 3 lower than the  $150\text{-}\mu\text{m/s}$ -limit of Sec. II E that marks the validity of the applied effective thermoviscous model.

In conclusion, the example highlights two important aspects: (1) The effective thermoviscous model enables 3D thermoviscous simulations in acoustofluidic systems, and (2) even moderate thermal gradients may create high streaming velocities in acoustofluidic systems. Such gradients can of course be created not only by heat generation in the transducer as in this example, but also more controllably by ohmic wires, Peltier elements, and external light sources. Notably, the validity of the perturbation approach breaks down at moderately high, but experimentally obtainable acoustic energy densities above  $\sim 100 \text{ J/m}^3$  in combination with a moderate thermal gradient  $\sim 1 \text{ K/mm}$ , and this calls for an extension beyond perturbation theory of the presented theory.

## VII. CONCLUSION

We have derived an effective thermoviscous theory for a fluid embedded in an elastic solid. The steady zeroth order temperature field is governed by Eq. (16). The acoustic fields are governed by the Helmholtz equations, Eqs. (19) and (23), the decompositions [Eqs. (20) and (24)], and the effective boundary conditions [Eq. (34)]. The time-averaged acoustic streaming is governed by the effective Stokes equation, Eq. (52), and the effective boundary conditions, Eq. (54). The theory includes the thermoviscous boundary layers and the acoustic temperature field  $T_1$  analytically, and impose them as effective boundary conditions and time-averaged body forces on the thermoacoustic bulk fields.

The theory has been implemented in a numerical model,<sup>21</sup> which, because it avoids resolving numerically the boundary layers, allows for simulating both the first-order thermoviscous acoustic fields and second-order steady fields in 3D models of acoustofluidic systems. A conventional

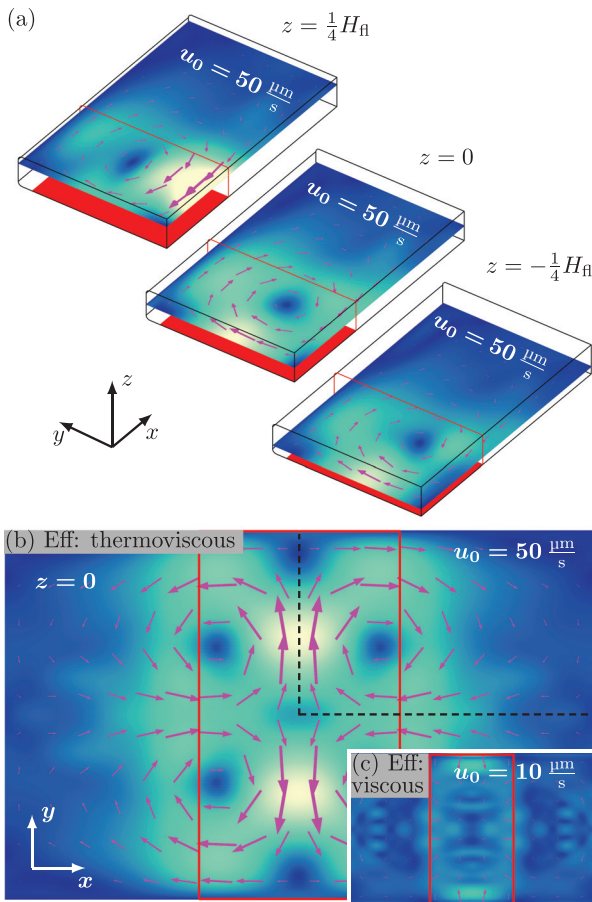


FIG. 4. (Color online) The streaming velocity  $v_2$  (magenta arrows) and its magnitude from 0 (blue) to  $u_0 = 50 \mu\text{m/s}$  (yellow) in a symmetry quarter of the trapping capillary tube. (a)  $v_2$  in three different horizontal planes. (b)  $v_2$  in the full central plane  $z = 0$ . The dashed black lines show the symmetry planes, and the red lines the edge of the actuation region. (c)  $v_2$  in the central plane  $z = 0$  without thermal effects. Note that here  $u_0 = 10 \mu\text{m/s}$ .

brute-force direct numerical simulations is very difficult due to large memory requirements. In 2D, the model was validated by direct numerical simulations, and in 3D, its self-consistency has been checked by mesh-convergence analyses.

We have applied the effective thermoviscous model in two numerical examples to demonstrate the importance of thermoviscous effects in microscale acoustofluidic devices. In particular, we have shown how the acoustic streaming depends strongly on the thermal fields: (1) The oscillating temperature field  $T_1$  impacts the streaming through the temperature dependency of the viscosity, causes corrections to the effective boundary condition, and spawns an additional body force in the bulk. In the 2D model of the square channel in Sec. VI A and Fig. 2, we have shown how the thermoviscous effects are particularly important for the morphology and magnitude of the streaming in a rotating acoustic field. (2) The presence of an inhomogeneous stationary temperature field  $T_0$  affects the streaming through the induced gradients in compressibility and density. In the 3D model of the capillary glass tube in Sec. VI B and Fig. 4, we have shown, how the experimentally-observed characteristic horizontal streaming rolls in the standing acoustic resonance of Fig. 3, are caused by heating from the actuation area. We have also shown, how very high streaming velocities ( $\sim 1$  mm/s) can be caused by small temperature gradients ( $\sim 1$  K/mm) for moderate acoustic energy densities ( $\sim 100$  J/m<sup>3</sup>).

Our theoretical model enables 3D simulations of thermoviscous effects in microscale acoustofluidic devices. The results point to new ways for microscale handling of fluids and particles using a combination of acoustic and thermal fields. Although we have developed the effective thermoviscous theory within the narrow scope of microscale acoustofluidics, it is more general and may find wider use in other branches of thermoacoustics.

## ACKNOWLEDGEMENTS

This work was supported by Independent Research Fund Denmark, Natural Sciences (Grant No. 8021-00310B).

<sup>1</sup>A. A. Doinikov, "Acoustic radiation force on a spherical particle in a viscous heat-conducting fluid. I. General formula," *J. Acoust. Soc. Am.* **101**(2), 713–721 (1997).  
<sup>2</sup>S. D. Danilov and M. A. Mironov, "Mean force on a small sphere in a sound field in a viscous fluid," *J. Acoust. Soc. Am.* **107**(1), 143–153 (2000).  
<sup>3</sup>J. T. Karlsen and H. Bruus, "Forces acting on a small particle in an acoustic field in a thermoviscous fluid," *Phys. Rev. E* **92**, 043010 (2015).  
<sup>4</sup>A. Y. Rednikov and S. S. Sadhal, "Acoustic/steady streaming from a motionless boundary and related phenomena: Generalized treatment of the inner streaming and examples," *J. Fluid. Mech.* **667**, 426–462 (2011).  
<sup>5</sup>P. B. Muller and H. Bruus, "Numerical study of thermoviscous effects in ultrasound-induced acoustic streaming in microchannels," *Phys. Rev. E* **90**(4), 043016 (2014).

<sup>6</sup>J. T. Karlsen, P. Augustsson, and H. Bruus, "Acoustic force density acting on inhomogeneous fluids in acoustic fields," *Phys. Rev. Lett.* **117**, 114504 (2016).  
<sup>7</sup>P. Augustsson, J. T. Karlsen, H.-W. Su, H. Bruus, and J. Voldman, "Iso-acoustic focusing of cells for size-insensitive acousto-mechanical phenotyping," *Nat. Commun.* **7**, 11556 (2016).  
<sup>8</sup>J. T. Karlsen and H. Bruus, "Acoustic tweezing and patterning of concentration fields in microfluidics," *Phys. Rev. Appl.* **7**, 034017 (2017).  
<sup>9</sup>J. T. Karlsen, W. Qiu, P. Augustsson, and H. Bruus, "Acoustic streaming and its suppression in inhomogeneous fluids," *Phys. Rev. Lett.* **120**(5), 054501 (2018).  
<sup>10</sup>W. Qiu, J. T. Karlsen, H. Bruus, and P. Augustsson, "Experimental characterization of acoustic streaming in gradients of density and compressibility," *Phys. Rev. Appl.* **11**(2), 024018 (2019).  
<sup>11</sup>J. S. Bach and H. Bruus, "Theory of pressure acoustics with viscous boundary layers and streaming in curved elastic cavities," *J. Acoust. Soc. Am.* **144**, 766–784 (2018).  
<sup>12</sup>N. R. Skov, J. S. Bach, B. G. Winkelmann, and H. Bruus, "3D modeling of acoustofluidics in a liquid-filled cavity including streaming, viscous boundary layers, surrounding solids, and a piezoelectric transducer," *AIMS Math.* **4**, 99–111 (2019).  
<sup>13</sup>N. R. Skov, P. Sehgal, B. J. Kirby, and H. Bruus, "Three-dimensional numerical modeling of surface-acoustic-wave devices: Acoustophoresis of micro- and nanoparticles including streaming," *Phys. Rev. Appl.* **12**, 044028 (2019).  
<sup>14</sup>J. S. Bach and H. Bruus, "Bulk-driven acoustic streaming at resonance in closed microcavities," *Phys. Rev. E* **100**, 023104 (2019).  
<sup>15</sup>L. D. Landau and E. M. Lifshitz, *Theory of Elasticity. Course of Theoretical Physics*, 3rd ed. (Pergamon Press, Oxford, UK, 1986), Vol. 7.  
<sup>16</sup>L. D. Landau and E. M. Lifshitz, *Fluid Mechanics*, 2nd ed. (Pergamon Press, Oxford, UK, 1993), Vol. 6.  
<sup>17</sup>L. D. Landau and E. M. Lifshitz, *Statistical Physics, Part 1*, 3rd ed. (Butterworth-Heinemann, Oxford, UK, 1980), Vol. 5.  
<sup>18</sup>A. Riaud, M. Baudoin, O. Bou Matar, J.-L. Thomas, and P. Brunet, "On the influence of viscosity and caustics on acoustic streaming in sessile droplets: An experimental and a numerical study with a cost-effective method," *J. Fluid Mech.* **821**, 384–420 (2017).  
<sup>19</sup>COMSOL, "COMSOL Multiphysics 5.6," <http://www.comsol.com> (30 March 2021).  
<sup>20</sup>M. W. H. Ley and H. Bruus, "Three-dimensional numerical modeling of acoustic trapping in glass capillaries," *Phys. Rev. Appl.* **8**, 024020 (2017).  
<sup>21</sup>See supplementary material at <https://www.scitation.org/doi/suppl/10.1121/10.0005005> for details on the material parameters and on the COMSOL implementation of geometry, mesh, PML, and effective and symmetry boundary conditions.  
<sup>22</sup>M. Antfolk, P. B. Muller, P. Augustsson, H. Bruus, and T. Laurell, "Focusing of sub-micrometer particles and bacteria enabled by two-dimensional acoustophoresis," *Lab Chip* **14**, 2791–2799 (2014).  
<sup>23</sup>P. Mishra, M. Hill, and P. Glynne-Jones, "Deformation of red blood cells using acoustic radiation forces," *Biomicrofluidics* **8**(3), 034109 (2014).  
<sup>24</sup>I. Gralinski, S. Raymond, T. Alan, and A. Neild, "Continuous flow ultrasonic particle trapping in a glass capillary," *J. Appl. Phys.* **115**(5), 054505 (2014).  
<sup>25</sup>B. Hammarström, T. Laurell, and J. Nilsson, "Seed particle-enabled acoustic trapping of bacteria and nanoparticles in continuous flow systems," *Lab Chip* **12**, 4296–4304 (2012).  
<sup>26</sup>J. Lei, P. Glynne-Jones, and M. Hill, "Acoustic streaming in the transducer plane in ultrasonic particle manipulation devices," *Lab Chip* **13**(11), 2133–2143 (2013).  
<sup>27</sup>H. Lei, D. Henry, and H. BenHadid, "Acoustic force model for the fluid flow under standing waves," *Appl. Acoust.* **72**(10), 754–759 (2011).  
<sup>28</sup>G. Werr, Z. Khaji, M. Ohlin, M. Andersson, L. Klintberg, S. S. Searle, K. Hjort, and M. Tenje, "Integrated thin film resistive sensors for *in situ* temperature measurements in an acoustic trap," *J. Micromech. Microeng.* **29**(9), 095003 (2019).  
<sup>29</sup>F. Collino and P. B. Monk, "Optimizing the perfectly matched layer," *Comput. Methods. Appl. Mech. Eng.* **164**(1-2), 157–171 (1998).